# Spatial orientation of nuclei: Mass deformation in 165-holmium

J. E. Koster,* C. R. Gould, and D. G. Haase
*North Carolina State University, Raleigh, North Carolina 27695*
*and Triangle Universities Nuclear Laboratory, Durham, North Carolina 27708*

N. R. Roberson
*Duke University, Durham, North Carolina 27708*
*and Triangle Universities Nuclear Laboratory, Durham, North Carolina 27708*
(Received 3 September 1993)

Measurements of neutron transmission through a rotating, cryogenically aligned holmium target are reported. From the variation in the transmission yield as a function of alignment angle we obtain holmium deformation cross sections of $-548 \pm 42$, $-354 \pm 17$, $-283 \pm 23$, and $248 \pm 23$ mb at neutron energies 1.5, 1.8, 1.9, and 3.9 MeV, respectively. Coupled channels calculations using deformed optical model parameters give a quadrupole mass deformation length $\beta_2 r_0 = 0.38 \pm 0.03$, consistent with the literature. In contrast to a recent result from analysis of pion single-charge-exchange scattering, the data imply similar deformation lengths for the proton and neutron distributions in holmium.

PACS number(s): 21.10.Gv, 25.40.Dn, 29.25.Pj, 27.70.+q

## I. INTRODUCTION

Determining nuclear shapes is a problem of continuing interest in nuclear physics. A particular issue relates to the question of whether the charge and mass distributions are the same in deformed nuclei. In the past, they have been considered to be identical. But in a recent pion charge exchange experiment, Knudson *et al.* [1] concluded that the quadrupole deformation of the neutrons in aligned $^{165}$Ho was $0.84 \pm 0.08$ that of the protons, implying significantly different charge and mass distributions.

In this paper we present measurements of neutron transmission through a rotating, cryogenically aligned single crystal $^{165}$Ho target. Whereas the pion charge exchange mechanism probes the neutron distribution, and electron scattering and muonic x-ray measurements probe the proton distribution, neutron total cross section measurements with an aligned target probe the combined mass distribution. The nuclei are spatially oriented inside the target and rotation of the target allows measurement of transmission yields through different axes of the nuclei. For deformed nuclei the yield changes as a function of alignment angle, and a deformation cross section can be determined. Coupled channels calculations are presented which fit the energy-dependent deformation effect. The experimental results are in agreement with previous measurements of the deformation effect in holmium [2–7]. Our calculations do not confirm the difference in proton and neutron deformations observed in the pion experiment.

Two previous nuclear physics experiments have used rotating aligned holmium targets. A 50 g cluster of 9 single crystals was rotated along with a polarizing magnet [8] in a study of the double-peaked giant dipole resonance. In Ref. [9], a single crystal of holmium ethyl sulfate, cooled to 0.29 K, was rotated so that the the optical anisotropy of holmium nuclei could be studied with 10–20 MeV $\gamma$ rays.

## II. HOLMIUM NUCLEAR ALIGNMENT

The nucleus $^{165}$Ho is highly deformed and relatively easy to align. Holmium is antiferromagnetic below 20 K [10], and at temperatures below 1 K, the large hyperfine interaction between the magnetically ordered electrons and the nuclei produces significant nuclear alignment in single crystals. The direction of orientation is 10° out of the $a$-$b$ plane of the hexagonal crystal structure. A turn angle of 30° exists between successive planes; the nuclear spins therefore form a spiral conical structure about the $c$ axis. In a crystal which has not been exposed to external magnetic fields, mirror domains cancel the component of magnetization along the $c$ axis.

The temperature dependence of the nuclear alignment is calculated from an effective Hamiltonian

$$E_m/k = -Am + P[m^2 - \tfrac{1}{3}I(I+1)] \,, \tag{1}$$

where $m$ is the magnetic substate quantum number of the $I = 7/2$ nuclear spin, $k$ is Boltzmann's constant, $A = 0.319$ K, and $P = 0.004$ K [11].

The degree of alignment $f_2$ is defined as

$$f_2 = [\langle m^2 \rangle - I(I+1)/3]/I^2 \,, \tag{2}$$

and for a target in thermal equilibrium, the expectation

*Present address: Los Alamos National Lab, Physics Division, Los Alamos, NM 87545.

 

value $\langle m^2 \rangle$ is given by

$$\langle m^2 \rangle = \sum_{m=-I}^{m=I} m^2 e^{-E_m/kT} \Big/ \sum_{m=-I}^{m=I} e^{-E_m/kT}. \quad (3)$$

To refer the alignment to arbitrary directions, it is convenient to replace $f_2$ by the statistical tensor $t_{20}(I)$ [12]. From the general relation for rank $K$,

$$t_{K0}(I) = I^K \hat{K} \hat{I} \sqrt{\frac{(2I-K)!}{(2I+K+1)!} \frac{(2K)!}{(K!)^2}} f_K, \quad (4)$$

with $\hat{K} = \sqrt{2K+1}$, we have $t_{20}(I) = 2.67 f_2$. The alignment with respect to the $c$ axis, $\hat{t}_{20}$, is given by a rotation of 80° out of the $a$-$b$ plane, that is,

$$\hat{t}_{20} = P_2(\cos 80°) t_{20}(I). \quad (5)$$

Typical temperatures during the experiment were 270 mK. This gives about 65% of the maximum $K = 2$ alignment, yielding $\hat{t}_{20} = 0.46$. In principle there are also $K = 4$ and higher alignments. But at this temperature $t_{40}(I)$ is only 28% of its maximum ($\hat{t}_{40} = 0.06$), and as discussed later, the effects of the higher rank alignments proved to be unobservable.

## III. DEFORMATION CROSS SECTIONS

The total cross section for a nucleus aligned at angle $\theta$ to the beam direction can be factored according to the statistical tensors describing the orientation:

$$\sigma_T(\theta) = \sum t_{K0}(\theta) \sigma_K. \quad (6)$$

For an aligned target with spin $I$ the sum goes over even values of $K \leq 2I$. The $\sigma_K$ for $K \geq 2$ are the deformation cross sections. The $t_{K0}$ here are statistical tensors describing the orientation of the target with respect to the beam direction. They are normalized to $t_{00} = 1$. All dependence on alignment axis angle and target temperature occurs in the statistical tensors $t_{K0}$, not in $\sigma_K$.

The $t_{K0}$ of Eq. (6) are referred to the beam direction, whereas the intrinsic alignments $\hat{t}_{K0}$ of Eq. (5) are referred to the $c$ axis. The values are related by

$$t_{K0}(\theta) = \hat{t}_{K0} d^K_{00} = P_K(\cos\theta) \hat{t}_{K0}, \quad (7)$$

where $d^K_{00}$ are the rotation matrices, and $P_K$ are Legendre polynomials.

As defined by Eq. (6), the deformation cross sections $\sigma_K$ are independent of the alignment of the target. This is convenient, but differs from previous work, where the deformation effect cross section $\Delta\sigma_{\rm def}$ (see, for example, Ref. [2]) is given by

$$\Delta\sigma_{\rm def} = t_{20}\sigma_2 + t_{40}\sigma_4 + \cdots . \quad (8)$$

The cross section in this form depends on the target temperature and alignment angle, and is therefore less useful for comparison to theoretical predictions.

## IV. EXPERIMENTAL APPARATUS

The experimental setup is shown in Fig. 1. The holmium target was a cylindrical single crystal of $^{165}$Ho, 99.8% purity, 2.29 cm in diameter, and 2.8 cm long, weighing 101.6 g. The crystal was grown by the Ames Laboratory Material Preparation Center at Iowa State University, and cut with the $c$ axis oriented radially. The $c$ axis was located precisely from x-ray diffraction.

The crystal was cooled to 270 mK in a dilution refrigerator constructed to search for a time reversal noninvariant contribution to the forward scattering amplitude in polarized neutron transmission [13,14]. The refrigerator provides a cooling power of 85 $\mu$W at 110 mK, reaching a no-load base temperature of 42 mK. It has a central shaft which connects a room temperature stepping motor to the copper coldfinger on which the target is mounted. The holmium cylinder is mounted vertically, allowing the alignment axis of the holmium single crystal to be rotated relative to the beam direction without changing the effective thickness of the target. The target was out-of-round by less than 4 parts in 10 000. The range of rotation was 270°, with a reproducibility of one-half of a degree.

The temperature of the holmium target was measured by two resistance thermometers mounted directly on the crystal. These thermometers were calibrated against a standard germanium resistance thermometer. It took 15 s to rotate through 90°. No heating of the target due to rotation was detected.

The neutron beam was produced by the $T(p,n)$ reaction. Protons from a direct extraction negative ion source were accelerated by the TUNL FN tandem Van de Graaff, and directed onto a 0.8 Ci/cm$^2$ tritiated titanium foil which was mounted on a 10 $\mu$g/cm$^2$ copper backing. The neutrons transmitted through the holmium were detected at zero degrees by a heavily shielded detector.

The detector consisted of a 12.7 cm thick, 12.7 cm diameter organic liquid scintillator and subtended a solid angle of 5 msr. Signals from the photomultiplier tube were pulse-shape analyzed to discriminate against gamma rays. The count of transmitted neutrons was normalized to the integrated proton beam current. Proton beams were typically 1 $\mu$A, resulting in neutron count rates of about 7000/s. The dead time in the electronics was about 3%. The background count rate was 30/h, determined by filling the collimator with 25 cm of polyethylene.

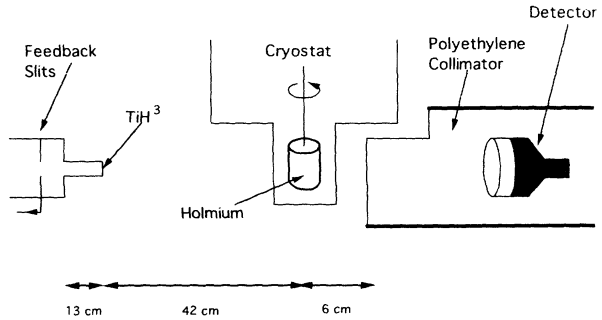


FIG. 1. Schematic of the experimental apparatus. The holmium target rotates about a vertical axis, and is cut in the shape of a cylinder with the $c$ axis pointing radially.

TABLE I. Experimental parameters for the four measurements of $\sigma_2(E)$.

| Incident neutron energy (MeV) | Degree of alignment | Number of runs used | Angle sequence Limits | Angle sequence Increment |
|---|---|---|---|---|
| 1.47 | 47% | 61 | ±90° | 30° |
| 1.84 | 67% | 49 | ±90° | 45° |
| 1.92 | 65% | 132 | ±135° | 45° |
| 3.88 | 60% | 42 | ±90° | 45° |

## V. EXPERIMENTAL PROCEDURE

The measurements were carried out at neutron energies of 1.47, 1.84, 1.92, and 3.88 MeV. As discussed later, the deformation effect cross sections change sign with energy, and these energies were chosen to give both positive and negative effects. The neutrons had a spread in energy of no more than 0.10 MeV, due largely to the thickness of the tritiated titanium foil. Important quantities for the measurements are summarized in Table I.

After cooling the sample, runs of $\approx$ 15 min duration were taken at each angle. Between runs the target was rotated by 30° or 45° to a new angle. Neutrons above a threshold of $\approx$ 1 MeV were counted in scalers which were read every 0.4 s. This provided a record of the transmission as a function of time for each run. Runs for which the proton beam current was unstable, or below a minimum value, were rejected. Data were also accumulated for a "warm" target ($T > 2.8$ K), in which the alignment is less than 2% of maximum.

The neutron yield in the detector has the following general form as a function of time $t$ and angle $\theta$ of alignment of the crystal:

$$N(\theta,t) = N_0(t)e^{-n_t\sigma_T(\theta,t)}, \tag{9}$$

$$\sigma_T(\theta,t) = \sigma_0 + P_2(\cos\theta)\hat{t}_{20}(t)\sigma_2 + P_4(\cos\theta)\hat{t}_{40}(t)\sigma_4. \tag{10}$$

We include at this stage terms up to $K = 4$. $N_0(t)$ is the time-dependent detector count per unit beam current and $n_t$ is the target thickness in atoms/b. In principle the target thickness varies across the beam because of the cylindrical shape. But if the neutron flux is uniform, the target thickness can be approximated by the average chord length through the cylinder. This approximation is good to better than 1% for our experiment [14], and in what follows we use an average thickness of $\pi d/4 = 1.80$ cm, giving $n_t = 0.06$ atoms/b.

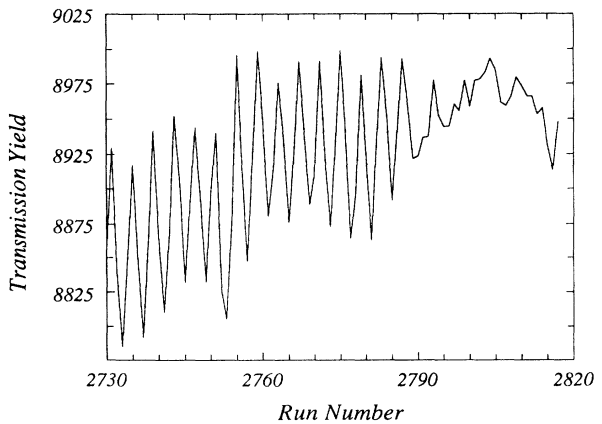


FIG. 2. Transmission yield for 1.8 MeV neutrons through a cold and a warm target (after run 2788). Each run corresponds to a different angle between the alignment axis and the beam direction. The sequence follows $\theta = 45°, 90°, 45°, 0°, -45°, -90°$ and back.

The 1.8 MeV transmission yields for target cold and target warm are plotted in Fig. 2. The run numbers correspond to the sequence of angles $\theta = 45°, 90°, 45°, 0°, -45°, -90°, \ldots$. The data for a cold sample show a clear oscillatory behavior, superimposed on a time-dependent drift. The phototubes were not gain stabilized, and so we expect the yield to vary slowly with time. The warm data show only the effects of gain drifts with time.

## VI. DATA ANALYSIS

Because the aligned target is rotated through a repeated sequence of orientations, it is possible to apply Fourier series techniques to the analysis of the data [15]. As shown in Fig. 2 the neutron yield is an oscillatory function of the run number $k$, as the crystal orientation is varied through a sequence of angles $\theta_k$. In our experiments several different sequences of $\theta_k$ were used. For example in Fig. 2 the cold target data consist of $n = 56$ runs in which the yield $N(\theta_k)$ oscillated through 14 complete periods. Each oscillation corresponds to the target rotating from 90°, to −90°, or −90° to 90°, in steps of 45°.

We can represent the neutron yield from the $k$th run as

$$x_k = \ln N(\theta_k) = \sum_{j=1}^{n} c_j e^{2\pi i \frac{(j-1)(k-1)}{n}}, \tag{11}$$

where $k = 1$ to $n$. This is a Fourier series expansion and the coefficients $c_j$ can be calculated from the Fourier series transform

$$c_j = \frac{1}{n}\sum_{k=1}^{n} x_k e^{-2\pi i \frac{(j-1)(k-1)}{n}}. \tag{12}$$

Because $x_k$ is real, this reduces to

$$c_1 = \frac{1}{n}\sum_{k=1}^{n} x_k \ ,$$

$$c_{2l-2} = \frac{1}{n}\sum_{k=1}^{n} x_k \cos\left[(k-1)(l-1)\frac{2\pi}{n}\right] \ ,$$

$$c_{2l-1} = \frac{1}{n}\sum_{k=1}^{n} (-x_k) \sin\left[(k-1)(l-1)\frac{2\pi}{n}\right] \ ,$$

$$c_n = \frac{1}{n}\sum_{k=1}^{n} (-1)^{k-1} x_k \ ,$$

where $l = 1, \ldots, n/2$. The deformation effect depends on $P_2 = \frac{1}{2}(3\cos^2\theta_k - 1) = \frac{1}{4}(3\cos 2\theta_k + 1)$ and is therefore reflected in the values of the $c_j$.

In Fig. 3 we show the $c_j$ determined from the cold target data of Fig. 2. The large $c_j$ found at $j = 28$ is the signature of the deformation effect. If the data set includes $m$ complete oscillations of the $+90°$ to $-90°$ and $-90°$ to $+90°$ sequence, the deformation effect is found at $j = 2m$. Here it also happens that $j = n/2$ because for $45°$ steps, the period is $n/m = 4$. The deformation effect cross section is given by $\sigma_2 = -8c_{28}/3n_t\hat{t}_{20}$. Consistent with the small $K = 4$ alignment, no peak is observed at $j = 56$ corresponding to a $P_4(\cos\theta)$ signal.

The large $c_j$ for $j$ small are due to slow drift in neutron yields which are uncorrelated with the target orientation. The drift can be removed from the yield data by setting these $c_j = 0$ and transforming the filtered $c_j$ back into $x_k$ by an inverse Fourier transform. The resultant filtered yields are shown in Fig. 4.

The final extraction of $\sigma_2$ and its associated statistical error was made by directly fitting to the logarithm of the filtered yield data of Fig. 4 as a function of angle. Neglecting terms in $K = 4$,

$$\ln N(\theta, t) = \ln(N_0 e^{-n_t\sigma_0}) - n_t P_2(\cos\theta)\hat{t}_{20}(t)\sigma_2, \quad (13)$$

which when plotted against $n_t P_2(\theta)\hat{t}_{20}(t)$ is a straight line with slope $\sigma_2$. The data are shown in Fig. 5, and the solid line is a linear least squares fit. The spread in the abscissa for each of the clusters of points is due to the fluctuations in temperature, and thus $\hat{t}_{20}$. The spread in the ordinate for each of the clusters arises from random fluctuation in repeated sampling of those values.

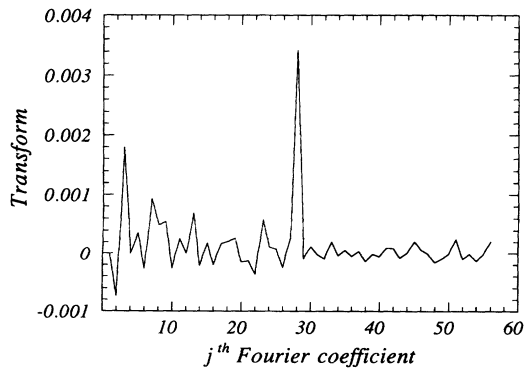


FIG. 3. Fourier transform of the data in Fig. 2. See text for definitions.

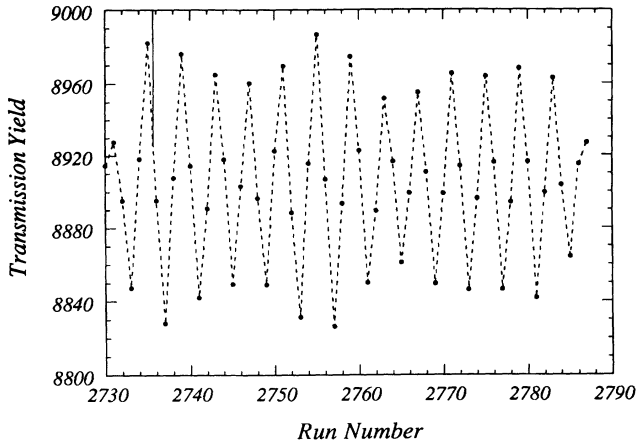


FIG. 4. Transmission yield of cold data at 1.8 MeV, after subtraction of long term gain drifts. The dotted line is a guide to the eye.

The results for the nuclear deformation effect $\sigma_2$ are summarized in Table II. A $\sigma_2$ was also extracted from three sets of data for an unaligned target (no such set was accumulated for the 1.9 MeV time reversal measurement.) These "warm" $\sigma_2$ values could in principle be nonzero due to geometric effects such as target out-of round or target wobble. However, the values are consistent with zero and no corrections were made for warm asymmetries in the final $\sigma_2$ values.

Although the $c$ axis was precisely located by x-ray diffraction, the deformation effect data can also be used to locate the alignment axis of the target crystal. A misalignment of the $c$ axis appears as an offset angle $\phi$ in Eq. (13), and shifts the phase of the oscillations in Fig. 4. We fit both the 1.8 and 3.9 MeV cold data sets, searching for the values of $\phi$ which minimized the $\chi^2$ in the least squares fits. We found $\phi$ to be $-1.5° \pm 3.1°$ consistent with zero [14].

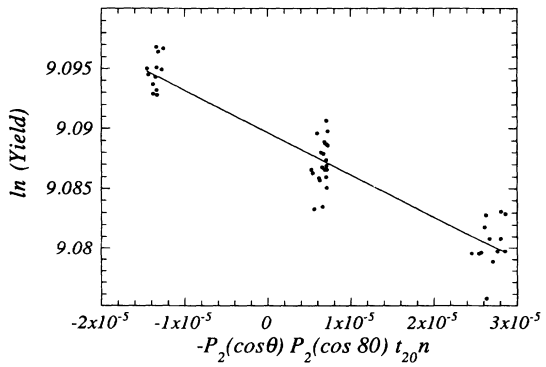


FIG. 5. Logarithm of 1.8-MeV transmission yield as a function of angle. The solid line is the linear least squares fit to the data.

TABLE II. Results of $\sigma_2$ measured as a function of incident neutron energy. The geometric $\sigma_2$ are seen to be consistent with zero and are not incorporated in $\sigma_2$.

| Neutron energy (MeV) | $\sigma_2$ (mb) | Warm target "$\sigma_2$" (mb) |
|---|---|---|
| 1.47 | $-548 \pm 42$ | $4 \pm 21$ |
| 1.84 | $-354 \pm 17$ | $14 \pm 13$ |
| 1.92 | $-283 \pm 23$ | – |
| 3.88 | $+248 \pm 23$ | $-1 \pm 10$ |

## VII. COMPARISON OF DEFORMATION EFFECT TO PREVIOUS EXPERIMENTS

The deformation effect in $^{165}$Ho has been measured previously, by comparing neutron transmission through an oriented and an unoriented target [2–7]. The present results are plotted against past measurements in Fig. 6. We report the effect in terms of the quantity $\sigma_2$ which is, as mentioned, independent of the degree of alignment. The previous measurements are renormalized by dividing by the $K = 2$ orientation attained. Some experiments used a polarized target where a small magnetic field is applied in the crystalline $a$-$b$ plane. The semimajor axis of the mass deformation is then in the $a$-$b$ plane—perpendicular to the $c$ axis. These data have been corrected by division by a geometric factor of $-1/2$.

Two data sets overlap our results. The present values are in good agreement with the high precision data of Fasoli *et al.* [3], but systematically slightly smaller than those of Marshak *et al.* [2], which also have larger statistical uncertainties.

## VIII. NUCLEAR DEFORMATION PARAMETERS

The shape deformation of a nucleus is described by an angle-dependent radius $R$ and deformation parameters $\beta_\lambda$:

$$R(\theta) = r_0 A^{1/3}\left(1 + \sum_{\lambda=2,4,6} \beta_\lambda Y_{\lambda 0}(\theta)\right). \tag{14}$$

Here $Y_{\lambda 0}$ are spherical harmonics. Our $\beta_\lambda$ are equivalent to the $\beta'_\lambda$ defined in Ref. [16], which reviews the common definitions. As in Ref. [17] the odd order $\beta_\lambda$ are assumed to be zero. The nuclear shape is then reflection symmetric with respect to the plane perpendicular to the axis of symmetry. The assumption of axial symmetry is common in this mass region [18]. Previous calculations for holmium did not include a hexacontatetrapole deformation $\beta_6$ although a small value was found helpful in reproducing $\alpha$-scattering data [19] on even-even rare earth nuclei, and in reproducing neutron scattering on tungsten isotopes [20].

The deformation effect cross sections $\sigma_K$ are given by [21]

$$\sigma_K = \mathrm{Re}\left\{2\pi\lambda\!\!\!^{-2}\hat{K}\sum_J g_J \sum_{ll'jj'} T_K(l'j'lj)[\delta_{ll'}\delta_{jj'} - S_J(lj \to l'j')]\right\}. \tag{15}$$

Here $g_J = (2J+1)/8$, $S_J$ is the $S$-matrix element for the transition from incoming channel $(lj)$ to outgoing channel $(l'j')$ and $T_K$ is a combination of angular momentum factors given by

$$T_K(l'j'lj) = (-1)^{s-l-j'}\hat{l}\hat{j}\hat{j}'\hat{I}\langle lK00|l'0\rangle W(JjIK;Ij')W(j'l'jl;sK), \tag{16}$$

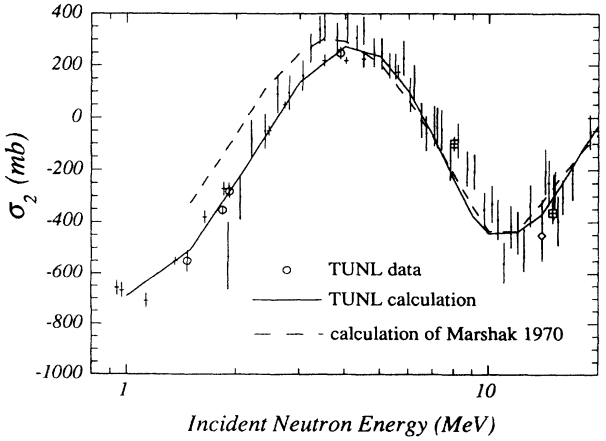


FIG. 6. Different sets of deformation cross sections, $\sigma_2(E)$. Key: open circles, present data; crosses [3]; solid squares [2]; asterisks [4]; crossed-box [5]; open diamond [6]; solid diamond [7]. The present calculation is given by the solid line. For comparison, the calculation in Ref. [2] is shown as the dashed line.

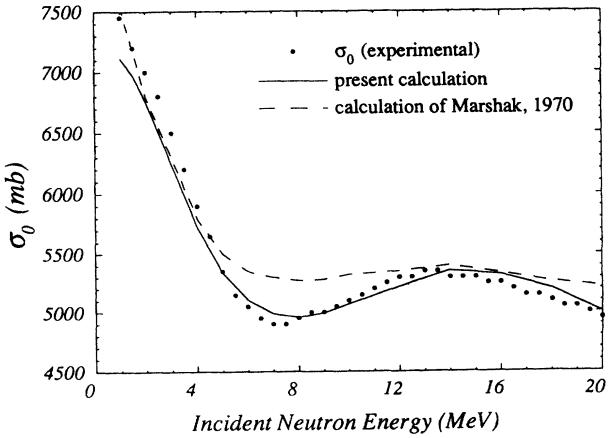


FIG. 7. The total cross section for neutrons on holmium. The data are from Ref. [26]. The present calculation is given by the solid line. For comparison, the calculation in Ref. [2] is shown as the dashed line.

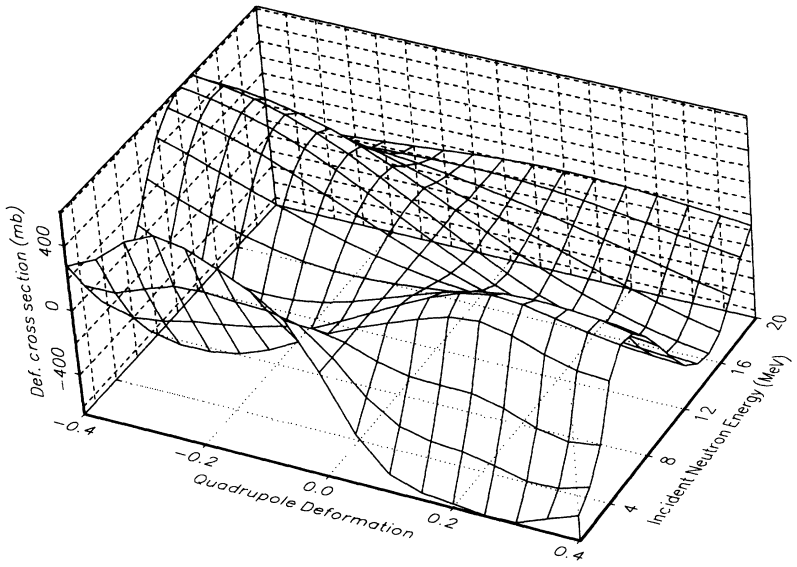


FIG. 8. The dependence of $\sigma_2$ on $\beta_2$ and the incident neutron energy.

The $S$-matrix elements $S_J$ were derived from a coupled channels calculation [22] using the code ECIS 89 [23]. The parameters for the deformed optical model were taken from calculations of Young *et al.* [24] for $^{165}$Ho and $^{169}$Tm. These calculations reproduced $s$- and $p$-wave neutron strength functions, total cross sections, and all available angular distributions. The first two excited states in $^{165}$Ho are coupled explicitly to the ground state. Imaginary potentials account for coupling to all other states.

Following Glendenning *et al.* [25], the optical model parameters are fixed in the present calculation and the deformation parameters are varied. The final $\beta_\lambda$ are those which result in the best fit to the experimental $\sigma_2(E)$ and the unpolarized target total cross section $\sigma_0(E)$ in the energy range 1–20 MeV [26].

The hexacontatetrapole deformation proved to have no effect on the deformation cross section at these energies and only very small effect on the total cross section. Setting $\beta_6 = 0$, we found the deformation parameters $\beta_2 = 0.30$ and $\beta_4 = -0.02$ of Young's parameter set [24] provided the best fits, as illustrated in Figs. 6 and 7. The agreement is much improved over the adiabatic coupled channels calculation in Ref. [2]. The optical model parameters are listed in Table III.

To determine how well the deformation effect data determine $\beta_2$, we show in Fig. 8 a plot $\sigma_2$ as a function of $\beta_2$ for neutron energies 1–20 MeV. In these calculations we fix $\beta_4 = -0.02$ at the value determined in the previous searches. We see the deformation cross section varies strongly with neutron energy and with deformation $\beta_2$. Figure 9 is a plot of $\sigma_2$ vs $\beta_2$ at a typical energy 3.9 MeV. For small $\beta_2$ ($|\beta_2| \leq 0.1$) the cross section grows linearly with deformation. For large $\beta_2$ the dependence is quite nonlinear, going through a maximum around $\beta_2 = 0.2$ and turning toward zero as $\beta_2$ increases.

As discussed earlier the most precise deformation effect data are our measurements values and the measurements of Fasoli *et al.* [3]. The two data sets are in good agreement with each other and cover the range between 1.5 and 4 MeV where there is a strong energy dependence as $\sigma_2$ crosses zero. We use these data to determine $\beta_2$ values at each energy by reading off from $\sigma_2$ vs $\beta_2$ plots as in Fig. 9. There will be no solution if statistical fluctuation

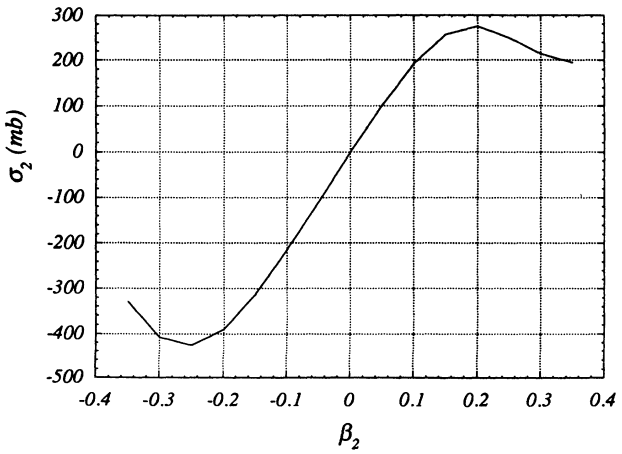


FIG. 9. The dependence of $\sigma_2$ on $\beta_2$ at 3.9 MeV. The cross section is proportional to $\beta_2$ in magnitude and sign only for $|\beta_2| \leq 0.1$.

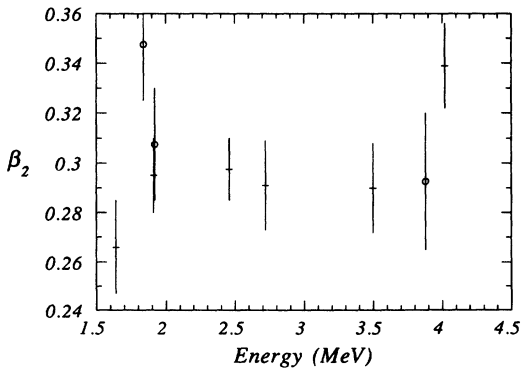


FIG. 10. Deformation parameters determined from the present $\sigma_2$ measurements (circles) and the $\sigma_2$ measurements of Ref. [3] (crosses) for neutron energies 1.5–4.0 MeV. A weighted average gives $\beta_2 = 0.30 \pm 0.025$.

TABLE III. Parameters for the deformed optical model calculation. The Woods-Saxon potentials are volume $V$, surface imaginary $W_D$, volume imaginary $W_V$, and spin orbit $V_{SO}$.

| Potential strength (MeV) | Radius (fm) | Diffuseness (fm) |
|---|---|---|
| $V = 49.8 - 16\frac{N-Z}{A} - 0.325E$ | 1.26 | 0.63 |
| $W_D(E \leq 6.5) = 5.0 - 8\frac{N-Z}{A} + 0.51E$ | 1.26 | 0.48 |
| $W_D(E > 6.5) = 8.3 - 8\frac{N-Z}{A} - 0.09(E - 6.5)$ | 1.26 | 0.48 |
| $W_V(E \leq 9.0) = 0.0$ | 1.26 | 0.63 |
| $W_V(E > 9.0) = -1.8 + 0.2E$ | 1.26 | 0.63 |
| $V_{SO} = 6.0$ | 1.26 | 0.63 |

TABLE IV. Quadrupole deformation lengths for the nucleon, proton, and neutron distributions in $^{165}$Ho.

| $\beta_2 r_0$ (fm) | Distribution | Reference |
|---|---|---|
| $0.38 \pm 0.03$ | nucleons | present experiment |
| $0.36 \pm 0.01$ | protons | [29] |
| $0.30 \pm 0.03$ | neutrons | [1] |

results in too large a value of $\sigma_2$. Usually there are two solutions. We consider the solutions close to $\beta_2 = 0.3$, as indicated in the previous calculations. The resulting $\beta_2$'s are plotted in Fig. 10 as a function of neutron energy. As expected the deformations are independent of energy. The weighted average is $\beta_2 = 0.30 \pm 0.025$, where the one-sigma uncertainty is determined from the spread of the values.

When comparing deformation parameters from different experiments, the reduced radius $r_0$ must be considered because cross sections scale with the deformation lengths $\beta_\lambda r_0$, rather than just deformation parameters. Deformation lengths $\beta_2 r_0$ from three different types of experiment are given in Table IV. Our deformation length is sensitive to the nucleon distribution, the muonic x-ray experiment of Ref. [27] is sensitive to the proton distribution, and the pion charge exchange experiment [1] is sensitive to the neutron distribution. For the present experiment $\beta_2 = 0.30 \pm 0.025$, and $r_0 = 1.26$ fm. For the muonic x-ray experiment $\beta_2 = 0.32 \pm 0.01$ and $r_0 = 6.15/165^{1/3} = 1.12$ fm. For the pion experiment the deformation length is the muonic x-ray value multiplied by $0.84 \pm 0.08$.

If we assume the deformation lengths are related by

$$(\beta_2 r_0)_{\text{nucleons}} = \frac{Z}{A}(\beta_2 r_0)_{\text{protons}} + \frac{N}{A}(\beta_2 r_0)_{\text{neutrons}} , \quad (17)$$

we can use our value and the precise charge distribution value to infer a neutron quadrupole deformation length. We find $(\beta_2 r_0)_{\text{neutrons}} = 0.39 \pm 0.05$ fm, which is to be compared to the value of $0.30 \pm 0.03$ inferred from Ref. [1]. Although the uncertainties are large, the present data in combination with the muonic x-ray data do not confirm the difference in neutron and proton deformations seen in the pion charge exchange data.

## IX. SUMMARY

We have measured the nuclear deformation effect in a single crystal, cryogenically aligned $^{165}$Ho target. Neutron transmission through different axes of the nuclei was accomplished by rotating the target, and a deformation cross section $\sigma_2$ was extracted from the angle dependence of data.

The total cross section and deformation cross section between 1 and 20 MeV were reproduced using coupled channels calculations and a deformed optical model potential. A quadrupole mass deformation length of $\beta_2 r_0 = 0.38 \pm 0.03$ was obtained, similar to the value obtained in muonic x-ray measurements of the holmium charge distribution. This implies similar proton and neutron deformations for $^{165}$Ho, in contrast to a recent analysis of data from pion charge exchange scattering.

## ACKNOWLEDGMENTS

We thank J.-P. Delaroche and V. Hnizdo for helpful discussions. We thank P. J. Young for providing his optical model parameter sets for holmium. We thank X. Zhu, W. S. Wilburn, C. D. Keith, and P. Huffman for help in taking data and for performing calculations. This work was supported in part by the U. S. Department of Energy, Office of High Energy and Nuclear Physics, under Contracts Nos. DE-AC05-76ER01067 and DE-FG05-88ER40441.

[1] J. N. Knudson, J. D. Bowman, S. I. Penttilä, J. R. Comfort, B. G. Ritchie, J. Goergen, D. Mathis, J. Tinsley, S. S. Hanna, B. King, D. Počanić, R. A. Loveman, L. S. Fritz, and N. S. Dixon, Phys. Rev. Lett. **66**, 1026 (1991).

[2] H. Marshak, A. Langsford, T. Tamura, and C. Y. Wong, Phys. Rev. C **2**, 1862 (1970).

[3] U. Fasoli, G. Galeazzi, D. Toniolo, and G. Zago, Lett. Nuovo Cimento **6**, 485 (1973).

[4] J. S. McCarthy, T. R. Fisher, E. G. Shelley, R. S. Safrata, and D. Healey, Phys. Rev. Lett. **20**, 502 (1968).

[5] T. R. Fisher, R. S. Safrata, E. G. Shelley, J. McCarthy, S. M. Austin, and R. C. Barrett, Phys. Rev. **157**, 1149 (1967).

[6] H. Marshak, A. C. B. Richardson, and T. Tamura, Phys.

Rev. **150**, 996 (1966).
[7] R. Wagner, P. D. Miller, T. Tamura, and H. Marshak, Phys. Rev. **139**, B29 (1965).
[8] M. A. Kelly, B. L. Berman, R. L. Bramblett, and S. C. Fultz, Phys. Rev. **179**, 1194 (1969).
[9] E. Ambler, E. G. Fuller, and H. Marshak, Phys. Rev. **138**, B117 (1965).
[10] W. C. Koehler, J. W. Cable, M. K. Wilkinson, and E. O. Wollan, Phys. Rev. **151**, 414 (1966).
[11] M. Krusius, A. C. Anderson, and B. Holström, Phys. Rev. **177**, 910 (1969).
[12] M. Simonius, *Polarization Nuclear Physics*, edited by D. Fick, Lecture Notes in Physics, Vol. 30 (Springer-Verlag, Berlin, 1974).
[13] J. E. Koster, E. D. Davis, C. R. Gould, D. G. Haase, N. R. Roberson, L. W. Seagondollar, S. Wilburn, and X. Zhu, Phys. Lett. B **267**, 23 (1991).
[14] J. E. Koster, C. R. Gould, D. G. Haase, N. R. Roberson, and L. W. Seagondollar, Nucl. Instrum. Methods A **313**, 464 (1992).
[15] T. W. Anderson, *The Statistical Analysis of Time Series* (Wiley and Sons, New York, 1971).
[16] K. E. G. Löbner, M. Vetter, and V. Hönig, Nucl. Data Tables A **7**, 495 (1970).
[17] R. Bengtsson, J. Dudek, W. Nazarewicz, and P. Olanders, Phys. Scr. **39**, 196 (1989).
[18] W. Nazarewicz, M. A. Riley, and J. D. Garrett, Nucl. Phys. **A512**, 61 (1990).
[19] D. L. Hendrie, N. K. Glendenning, B. G. Harvey, O. N. Jarvis, H. H. Duhm, J. Saudinos, and J. Mahoney, Phys. Lett. **26B**, 127 (1968).
[20] J. P. Delaroche, Phys. Rev. C **26**, 1899 (1982).
[21] C. R. Gould, D. G. Haase, N. R. Roberson, H. Postma, and J. D. Bowman, Int. J. Mod. Phys. A **5**, 2181 (1990).
[22] Taro Tamura, Rev. Mod. Phys. **17**, 679 (1965).
[23] J. Raynal, Technical Report No. IAEA-SMR-9/8, International Atomic Energy Agency, 1970, ECI589 (unpublished).
[24] P. G. Young, E. D. Arthur, C. Philis, P. Nagel, and M. Collin, in *Nuclear Data for Science and Technology*, edited by K. H. Böckhoff (Reidel, Dordrecht, 1983), p. 792.
[25] N. K. Glendenning, D. L. Hendrie, and O. N. Jarvis, Phys. Lett. **26B**, 131 (1968).
[26] V. McLane, C. L. Dunford, and P. F. Rose, *Neutron Cross Section Curves* (Academic Press, Boston, 1988).
[27] R. J. Powers, F. Boehm, P. Vogel, A. Zehnder, T. King, A. R. Kunselman, P. Roberson, P. Martin, G. H. Miller, R. E. Welsh, and D. A. Jenkins, Phys. Rev. Lett. **34**, 492 (1975).

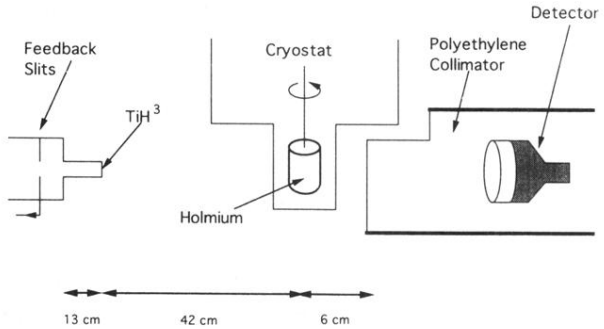


**FIG. 1. Schematic of the experimental apparatus. The holmium target rotates about a vertical axis, and is cut in the shape of a cylinder with the *c* axis pointing radially.**